A Mass Flux Model of Nocturnal Cold-Air Intrusions into a Closed Basin

Thomas Haiden

Central Institute for Meteorology and Geodynamics, Vienna, Austria

C. David Whiteman, Sebastian W. Hoch, and Manuela Lehner

University of Utah, Salt Lake City, Utah

ABSTRACT

Observations made during the Meteor Crater Experiment (METCRAX) field campaign revealed unexpected nighttime cooling characteristics in Arizona's Meteor Crater. Unlike in other natural closed basins, a near-isothermal temperature profile regularly develops over most of the crater depth, with only a shallow stable layer near the crater floor. A conceptual model proposed by Whiteman et al. attributes the near-isothermal stratification to the intrusion, and subsequent detrainment, of near-surface air from outside the crater into the crater atmosphere. To quantify and test the hypothesis, a mass flux model of the intrusion process is developed. It is found that the observed temperature profile can be reproduced, providing confirmation of the conceptual model. The near-isothermal stratification can be explained as a result of progressively cooler air entering the crater and detraining into the atmosphere, combined with the finite time of ascent in the compensating rising motion. The strength of detrainment largely determines the characteristics of the cooling process. With weak detrainment, most of the cooling arises from an adiabatic rising motion ("filling-up" mode). Stronger detrainment leads to reduced rising motion and enhanced cooling at upper levels in the crater ("destabilization" mode). Of interest is that the detrainment also reduces the total cooling, which, for a given intrusion mass flux, is determined by the temperature difference between the intruding air and the crater atmosphere at rim height.

1. Introduction

In closed basins, nighttime cooling frequently leads to the formation of pronounced inversions. The convergence of thermally driven downslope flows provides rapid initial cooling and the formation of a stable stratification at the basin floor. This stable stratification, combined with the confined geometry of the closed basin, which provides efficient sheltering with respect to the ambient flow, allows the in situ surface-driven cooling to remain concentrated in a shallow layer. Under favorable conditions, record minimum temperatures may occur at the floor of such basins. Temperature inversions of 10–15 K between the floor and the rim of the basin (over a depth on the order of 100 m) are common, and 30 K can be observed in more extreme cases.

In 2006, the Meteor Crater Experiment (METCRAX) field campaign was conducted in Arizona's Meteor Crater (Whiteman et al. 2008). Measurements were designed to elucidate the mechanisms important in the buildup and destruction of the nighttime inversions. Unlike previously studied sinkhole basins (Clements et al. 2003; Whiteman et al. 2004; Steinacker et al. 2007), the Meteor Crater is to a good approximation rotationally symmetric and does not have any higher-elevation drainage areas. It was considered an ideal site for studying the undisturbed buildup of nighttime inversions. The temperature evolution, however, was found to be fundamentally different from that in previously studied basins of comparable size (Whiteman et al. 2008). While there was continuous cooling, a near-isothermal stratification persisted throughout the night in much of the crater atmosphere (Fig. 1). A surface-based strong stability layer was present only in the lowest 20% of the crater atmosphere. This behavior was observed during several nights and represented a recurring, systematic phenomenon. On the basis of the available data, a conceptual

Corresponding author address: C. David Whiteman, Dept. of Atmospheric Sciences, University of Utah, 135 S 1460 E, Rm. 819, Salt Lake City, UT 84112-0110.
E-mail: dave.whiteman@utah.edu

model was proposed (Whiteman et al. 2010). The conceptual model states that cold air that forms on the slightly sloping mesoscale plain outside the crater (Savage et al. 2008) interacts with the crater topography. While part of the flow splits around the crater, an upper portion is lifted up the crater rim, flows down the inner sidewall of the crater, and leads to a cooling pattern that is different from what would be expected from purely local cooling.

In this paper the conceptual picture suggested by Whiteman et al. (2010) is tested within the framework of a mass flux model, which is solved analytically and numerically. The central questions we would like to answer are (i) whether an intrusion of cold air from the outside can cause the basin atmosphere to become near-isothermal, and (ii) what mechanism causes the isothermalcy.

The problem addressed in this study is of interest also in the wider context of basin and valley meteorology. Decoupling of the surface layer from the flow aloft and the formation of cold-air pools occur frequently in complex terrain. The influence of synoptic or mesoscale flows on persistent cold-air pools in large basins and valleys has been investigated by Whiteman et al. (1999), Zhong et al. (2001), Zängl (2005a,b), and Reeves and Stensrud (2009), among others. These studies show the importance of cold-air advection, as compared to turbulent erosion, radiation, and other mechanisms, in the dissipation of cold-air pools. In small-scale basins, where more complete datasets are available from field studies, the process of mixing-induced *warm* intrusions and their effect on inversion development has been documented (Eisenbach et al. 2003). The peculiar phenomenon of mesoscale *cold-air* intrusions in the case of the Meteor Crater offers a small-scale analog to the cold-air advection in larger basins, which in this way can be investigated in more detail.

The paper is organized as follows: section 2 presents the mass flux model and some analytical solutions for the simplified case of intrusion-only cooling. The combined effect of in situ and intrusion cooling is investigated numerically in section 3. The physical significance of the near-isothermal stratification is discussed, and the effect of incomplete mixing of detrained air is studied.

2. Mass flux model

a. Model equations

To understand how cold-air intrusions affect the temperature evolution inside a closed basin, a mass flux and heat budget model is formulated. The hypothesis to be tested is that such intrusions can lead to a near-isothermal stratification above a strongly stratified surface layer. To reduce the problem to its essentials and make an analytical
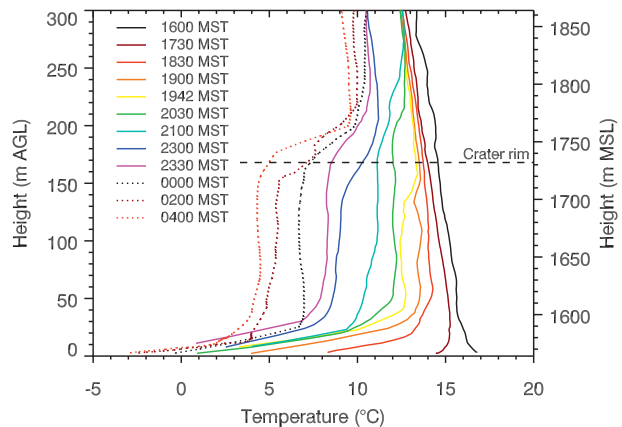

FIG. 1. Example of a sequence of tethered balloon soundings from the floor of Arizona's Meteor Crater, 22–23 Oct 2006.

solution possible, we first consider a two-dimensional basin geometry with vertical sidewalls. In a further step we take into account the actual topography of the Meteor Crater.

The mass flux approach is most commonly used in the parameterization of both moist and dry atmospheric convection in numerical models (e.g., Emanuel 1991; Hourdin et al. 2002; Fletcher and Bretherton 2010). It has also been useful in the assessment of bulk effects of thermally driven flows in complex terrain (Manins and Sawford 1979; Mahrt 1982; Freytag 1987; Haiden and Whiteman 2005), where the fully three-dimensional flow structure is usually not known. It is particularly useful in closed basins, where conservation of mass requires that the upward mass flux equals the downward mass flux at any level at any time. For the two-dimensional geometry and notation given in Fig. 2, this can be written

$$M = UD = w(L - D) \approx wL, \tag{1}$$

where w is the rising motion in the bulk of the crater atmosphere, U is the downward motion inside the katabatic intrusion layer, and M is the kinematic mass flux. In this paper we use the term mass flux for M, keeping in mind that it is actually a volume flux. The mass flux and volume flux are proportional, with the constant of proportionality being atmospheric density. Since the flow is shallow compared to the scale height of the atmosphere, density is assumed constant. Also, typically $D \ll L$ by almost two orders of magnitude, so the near-equality on the rhs of (1) is a good approximation.

Cold air entering the crater because of its negative buoyancy must to some extent detrain into the crater interior because of interfacial mixing, thereby cooling the crater. As a consequence of the detrainment, the vertical mass flux decreases downward. At some height the flow
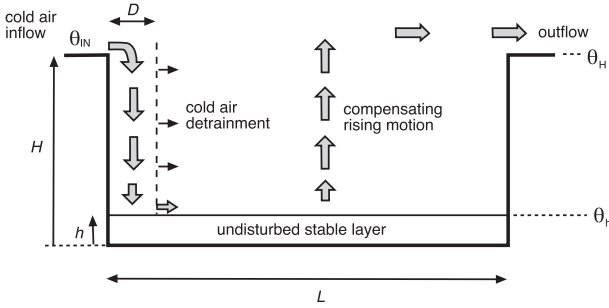
FIG. 2. Schematic representation of the cold-air intrusion process, leading to direct cold-air detrainment and adiabatic cooling due to a compensating rising motion.

may reach its level of neutral buoyancy (LNB) h, where the remaining cold air detrains completely. It should be pointed out that the more general concept of buoyancy sorting and detrainment has been developed for mass flux parameterizations of moist convection (Emanuel 1991), where evaporatively cooled mixtures of cloudy and dry air descend to, and detrain at, their LNB. In a similar vein we present a more general version of the intrusion model in section 3g, allowing for a range of LNBs associated with different mixtures of intrusion and crater air.

Because of the very low moisture content of the air at the Meteor Crater, the effect of humidity on buoyancy can be neglected. During the night of 22–23 October 2006 (the temperature evolution of which is shown in Fig. 1), specific humidity values outside and in the crater were within the range of 2.2–2.7 g kg^{-1}. Specific humidity differences between inflowing and crater air did not exceed 0.2 g kg^{-1}, giving a contribution to buoyancy of less than 0.04 K.

Compensating rising motion cools the crater adiabatically. The outflow mass flux over the downwind rim must equal the inflow mass flux. For the crater as a whole, the cooling due to the process can be written

$$L \int_h^H \frac{\partial \theta}{\partial t} \, dz = M_{IN}[\theta_{IN} - \theta(H)], \qquad (2)$$

where $z = 0$ at the crater floor and H is the depth of the crater. The subscript IN denotes inflow conditions, and $M_{IN} = U_{IN} D_{IN}$. Equation (2) states that there is cooling whenever the inflowing air is colder than the air at rim level inside the crater. From (2) it follows that the time scale of the bulk cooling is

$$\tau_{BULK} = \frac{L(H - h)}{U_{IN} D_{IN}}. \qquad (3)$$

For parameter values typical of the Meteor Crater ($L = 1200$ m, $H - h = 170$ m, $U_{IN} = 2$ m s^{-1}, and $D_{IN} = 10$ m), a cooling time scale of $\sim$3 h is obtained. This is comparable

to the e-folding time of normal surface-driven cooling in sinkholes, which is typically 2–3 h (Whiteman et al. 2004; DeWekker and Whiteman 2006). Thus the intrusion mechanism has the potential of being a major factor in nighttime cooling in such basins.

To understand how the intrusions affect the vertical profile of cooling, the contributions of detrainment and adiabatic rising motion at each level need to be formulated explicitly. Based on dimensional considerations and on the fact that the mixing is shear induced, detrainment is parameterized as

$$\frac{dM}{dz} = \frac{d}{dz}(DU) = C_D U, \qquad (4)$$

where C_D is a nondimensional detrainment coefficient. It is assumed that the decrease of M along the slope is mainly associated with a decrease of U, whereas D remains roughly constant. This assumption is based on the laboratory results of Baines (2001), which show that after an initial adaptation region the downslope flow reaches a quasi-equilibrium depth. From (4), one obtains an exponential decrease of mass flux down the slope:

$$M(z) = M_{IN} \exp\left[\frac{C_D}{D}(z - H)\right]. \qquad (5)$$

Using (1), the associated rising motion in the crater atmosphere can be written

$$w(z) = \frac{M_{IN}}{L} \exp\left[\frac{C_D}{D}(z - H)\right]. \qquad (6)$$

Changes of temperature $\theta(z, t)$ of the crater atmosphere due to cold-air intrusions are governed by the budget equation

$$\frac{\partial \theta}{\partial t} = -\frac{\partial}{\partial z}[w(\theta - \theta_{IN})] = -w\frac{\partial \theta}{\partial z} - (\theta - \theta_{IN})\frac{\partial w}{\partial z}, \qquad (7)$$

where the first term on the right-hand side is adiabatic cooling due to the compensating rising motion, and the second term is direct detrainment cooling. The temperature θ_{IN} of the inflowing air is not a function of z, but may vary over time. Using the total derivative, (7) can be written as

$$\frac{d\theta}{dt} = -\frac{(\theta - \theta_{IN})}{\tau_D} \exp\left[\frac{C_D}{D}(z - H)\right], \qquad (8)$$

where a detrainment time scale $\tau_D \equiv L/(C_D U_{IN})$ has been defined. If z in (8) is expressed as a function of the initial coordinate z_0 and time t, the problem can be reduced from a partial to an ordinary differential

equation, which can be solved analytically by using a Lagrangian framework (z_0, t) and then transforming the solution back to the Eulerian system (z, t).

b. Analytical solution of intrusion cooling

The first step is to determine the location of a parcel as a function of initial location and time $z(z_0, t)$. From $w = dz/dt$ and (6) it follows that

$$t = \int_0^t dt = \int_{z_0}^z \frac{dz}{w(z)} = \frac{L}{M_{IN}} \int_{z_0}^z \exp\left[\frac{C_D}{D}(H - z)\right] dz. \tag{9}$$

Integration of (9) gives, after some rearranging,

$$z(z_0, t) = H - \frac{D}{C_D} \ln\left\{\exp\left[\frac{C_D}{D}(H - z_0)\right] - \frac{t}{\tau_D}\right\}. \tag{10}$$

Inserting (10) into (8) gives

$$\frac{d\theta}{\theta_{IN} - \theta} = \frac{1}{\tau_D} \frac{dt}{\exp\left[\frac{C_D}{D}(H - z_0)\right] - \frac{t}{\tau_D}}, \tag{11}$$

which can be integrated to

$$\ln|\theta_{IN} - \theta| = \ln\left|\exp\left[\frac{C_D}{D}(H - z_0)\right] - \frac{t}{\tau_D}\right| + c. \tag{12}$$

The integration constant c is determined from the initial condition $\theta(z_0, 0) = \theta_0(z_0)$. This leads to

$$\theta(z_0, t) = \theta_{IN} + [\theta_0(z_0) - \theta_{IN}]\left\{1 - \frac{t}{\tau_D} \exp\left[\frac{C_D}{D}(z_0 - H)\right]\right\}, \tag{13}$$

which, by using (10), can also be written

$$\theta(z_0, z) = \theta_{IN} + [\theta_0(z_0) - \theta_{IN}] \exp\left[\frac{C_D}{D}(z_0 - z)\right]. \tag{14}$$

The time evolution of the vertical temperature profile $\theta(z, t)$ is obtained by again using (10), to express z_0 as a function of z and t,

$$z_0(z, t) = H - \frac{D}{C_D} \ln\left\{\exp\left[\frac{C_D}{D}(H - z)\right] + \frac{t}{\tau_D}\right\}, \tag{15}$$

and inserting it into (13) or (14). In the actual computation of the solution, it must be taken into account that the inflow is assumed not to penetrate past its LNB

defined by $\theta_{IN} = \theta_0(h)$. This is achieved by setting $z_0 = h$ whenever there would be $z_0 < h$ according to (15).

The solution obtained so far, as given by (13) and (15), represents intrusion cooling only and thus cannot be expected to closely match observations in the real atmosphere, where in situ cooling takes place as well. However, during the night of 26–27 October 2006 an unusually late cold-air intrusion was observed in the Meteor Crater, after the stratification had already reached $d\theta/dz \approx 0.04$ K m^{-1} (Whiteman et al. 2010, their Fig. 6). We use this value as an initial stratification. Based on observations of the magnitude of temperature drop at rim level on the upwind side of the crater, as indicated in the Whiteman et al. (2010) figure, we set the initial temperature deficit of the inflowing air to 5 K. The other model parameters are set as before, that is, $L = 1200$ m, $H - h = 170$ m, and $D_{IN} = 10$ m.

Figure 3 shows that the crater atmosphere reacts quickly to the cold-air intrusion. The evolution of the temperature profile assumes different forms depending on the strength of detrainment. (Note that in all figures temperature rather than potential temperature is shown, to make identification of isothermalcy easier.) If C_D is small, most of the cooling is due to lifting, which creates a sequence of almost linear profiles above an adiabatic layer growing from the LNB upward. This mode of cooling is similar to a filling-up process, like liquid poured into a container (Fig. 3a). If C_D gets bigger, more of the cooling is taking place at upper levels, creating curved temperature profiles (Figs. 3b,c). Mathematically, the curvature can become so strong that a superadiabatic stratification develops. There is no physical mechanism in the above equations that would inhibit that. In the real atmosphere, buoyancy-driven mixing would quickly remove such unstable gradients. The simplest way to model this would be by using dry-adiabatic adjustment. This method has been used in the numerical model described below. However, a closed analytical solution is then no longer possible.

It can be seen from Fig. 3 that the bulk cooling after a given time differs in the three cases shown. The strength of detrainment not only determines the partitioning between the detrainment and lifting contributions, but also influences the total amount of cooling. This is because the net cooling depends not just on the temperature of the inflowing air but on the temperature difference between inflowing and outflowing air [(2)]. For a given temperature of the inflowing air (in contrast to a given temperature deficit), the cooling is stronger if the air at upper levels in the crater remains warmer. One could imagine a (hypothetical) extreme case with a very large value of C_D, where all the cooling takes place in the uppermost layer. The temperature of this layer would drop rapidly to
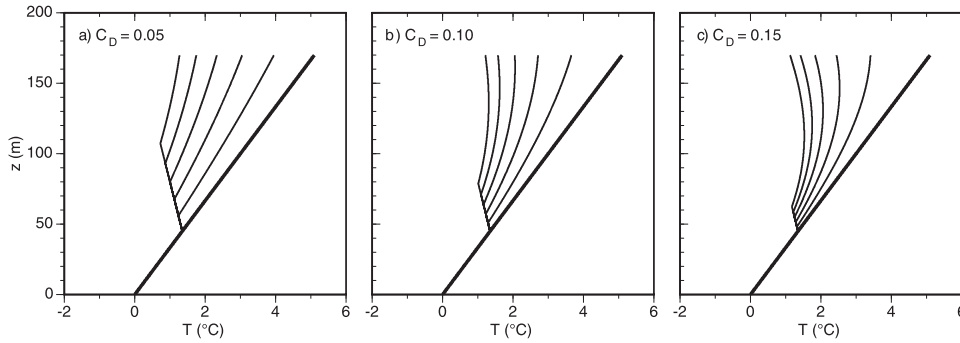
FIG. 3. Analytical solution of intrusion-only cooling as given by (13) and (15) for increasing detrainment strength: C_D = (a) 0.05, (b) 0.10, and (c) 0.15. Stronger detrainment leads to increased cooling at upper levels and reduced adiabatic upward motion. The initial temperature deficit of the inflowing air is 5 K, which in this case gives an LNB of 45 m. Time step between curves is 20 min; initial state is given by the thick line.

a value close to the temperature of the inflowing air, and little further cooling would occur. In reality, vertical mixing removes unstable gradients, so that the lowest possible temperature in the uppermost layer, and thus the smallest intrusion cooling, would be one corresponding to a dry-adiabatic stratification.

3. Numerical model results

a. Parameterization of in situ cooling

The cooling due to the cold-air inflow, if given sufficient time, evidently leads to a dry-adiabatic temperature profile. In the real atmosphere there is the additional surface-driven cooling, which tends to increase stability. We now investigate under which conditions the combined effect of both processes results in a near-isothermal temperature profile.

The in situ surface-driven cooling rate is parameterized by

$$
\left(\frac{\partial \theta}{\partial t}\right)_{\text{INSITU}} = \frac{H_{\text{SFC}}(t)}{c_p \rho} \times \begin{cases} \dfrac{\exp\left(-\dfrac{z}{b}\right)}{b\left[1 - \exp\left(-\dfrac{H}{b}\right)\right]} & t < t_I \\[12pt] \dfrac{2}{H}\left(1 - \dfrac{z}{H}\right) & t \geq t_I, \end{cases}
$$
(16)

where it is assumed that the surface sensible heat flux decreases exponentially in the course of the night (Whiteman et al. 2004) according to

$$
H_{\text{SFC}}(t) = H_{\text{SFC}}(0) \, \exp\left(-\frac{t}{\tau_{\text{SFC}}}\right),
$$
(17)

with $H_{\text{SFC}}(0) = -40$ W m^{-2} and $\tau_{\text{SFC}} = 6$ h. Formulation (16) represents a cooling that decreases exponentially with height for times earlier than t_I, which is the

time of onset of the inflow, typically ~2 h. After that, the strength of the surface inversion at the basin floor does not increase further but the whole basin atmosphere stabilizes. This is given by the linear, second part of (16). In both cases the total cooling rate integrated over the depth H of the basin has been normalized to equal $H_{\text{SFC}}(t)/(c_p \rho)$. The value of the depth scale parameter b (=15 m) has been chosen to match the observed cooling in the crater *before* the onset of the cold-air inflow. The general form of the parameterization is based on observations of the surface sensible heat flux and temperature evolution in closed basins (Clements et al. 2003; Steinacker et al. 2007). According to these observations, the heat flux is on the order from -30 to -40 W m^{-2} at the beginning of the cooling process and decreases to almost negligible values during the course of the night. The decrease in heat flux is due to turbulence suppression by the increasing stratification associated with reduced outgoing net surface radiation and increased soil heat flux as the surface gets significantly colder than both the air aloft and the deeper soil layers (Whiteman et al. 2004). At the beginning, a shallow surface inversion rapidly forms at the basin floor, while later on the bulk of the basin atmosphere undergoes cooling with little further strengthening of the surface inversion. Figure 4a shows the temperature evolution given by (16) and (17). Temperature observations made in the Meteor Crater during synoptically undisturbed conditions over a period of one month using lines of temperature data loggers running up the crater sidewalls confirm that the initial heat loss, taking into account the reduced volume of the crater, is equivalent to a surface sensible heat flux of -40 W m^{-2}. It decreases to about half this value within the next 4 h, and to about -10 W m^{-2} after another 4 h, corresponding to a negative-exponential time scale of $4[\ln(2)]^{-1} \approx 6$ h.
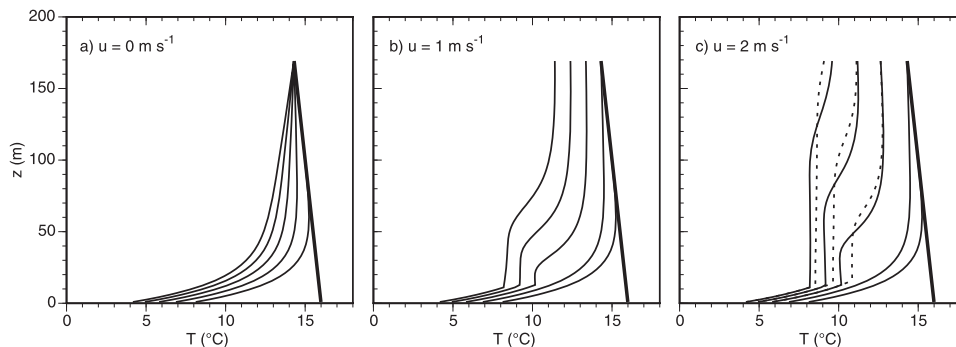
FIG. 4. Time evolution of temperature for cold-air inflow increasing (a) 0, (b) 1, and (c) 2 m s^{-1}, switched on at $t_I = 2$ h, and a value of the detrainment parameter of $C_D = 0.05$. In the cases with nonzero inflow, a quasi-linear, slightly stable profile develops above the stable surface layer. Time step between curves is 1 h; initial state is given by the thick line. Panel (c) shows the effect of including entrainment (dashed) for a value of the entrainment coefficient of $C_E = 0.02$.

Prescribing the in situ cooling enables us to focus on the phenomenon of the near-isothermal stratification but also limits the generality of some of our results. A unified treatment of the downslope flow driven by in situ cooling and the intruding flow would be more satisfying. However, one would also have to model the further cooling of air once it arrives at the crater floor and becomes virtually stagnant. The nonlocal nature of turbulence generation under strongly stratified conditions poses a challenge for mesoscale models that rely on Monin–Obukhov similarity theory (Pinto et al. 2006). Large-eddy simulations (LES) have been used with some success in the modeling of daytime thermally driven flows on small scales in complex terrain (Chow et al. 2006; Weigel et al. 2006). However, even in an LES model, nighttime downslope flows are difficult to represent because of their smaller depth, intermittent turbulence, and the generally smaller scale of energy-containing eddies in stable boundary layers.

b. Combined intrusion and in situ cooling

The combined intrusion and in situ cooling is modeled on the basis of (7), like in the case of the intrusion-only model, but solved numerically. The discretization consists of 100 layers in the vertical ($\Delta z = 1.7$ m), and the heat budget equation in (7) is used in flux form to ensure conservation of heat. To make the simulation results comparable to the observations on 22–23 October 2006 (Fig. 1), we start with a vertically uniform potential temperature corresponding to a temperature of 16°C at the basin floor. The intrusion cooling is not "switched on" immediately, but after 2 h of undisturbed in situ cooling. Thus after 2 h the profile is still the same in all cases. The outside air at rim level is assumed to have an initial temperature deficit at $t = 0$ of 1 K. Its temperature then decreases linearly over time at a rate of 1 K h^{-1}.

This rate is based on the observed decrease of temperature at the rim on 22–23 October 2006. All other model parameters are kept at the values used above.

Figure 4 shows the evolution of the temperature profile for the combined in situ and intrusion cooling for increasing values of inflow speed. It can be seen that a quasi-linear, near-isothermal layer develops above the stable surface layer. The complete formation of this quasi-linear layer takes a little more than 3 h in the case of stronger inflow (2 m s^{-1}). For weaker inflow (1 m s^{-1}) the quasi-linear layer develops as well, but after a proportionally longer time. Comparing Figs. 4b and 4c, it can be seen that the profile at 2 h after switch-on in the weak inflow case is similar to that at 1 h after switch-on in the stronger inflow case.

So far we have neglected entrainment into the intrusion flow, based on the observation that the near-surface, alongslope temperature profile at the upwind slope during intrusion events in the crater is close to dry-adiabatic. However, slightly superadiabatic profiles are sometimes seen (cf. Fig. 6 of Whiteman et al. 2010), which suggests that some mixing of warmer crater air into the colder air of the inflow may occur. Here we briefly investigate the effect on the temperature evolution of including entrainment in the model. In (4)–(6) for the downslope mass flux and compensating rising motion, C_D gets replaced by $C_D - C_E$, where C_E is the entrainment coefficient. In the heat budget equation in (7), the temperature of the intrusion now varies as $\theta_{IN} = \theta_{IN}(z)$, with the downward increase of θ_{IN} due to entrainment governed by

$$\frac{\partial \theta_{IN}}{\partial z} = \frac{C_E}{D}(\theta_{IN} - \theta). \qquad (18)$$

Here the local rate of change of θ_{IN} has been neglected. There is now a mutual dependence between θ and θ_{IN} in

the form of the coupled equations in (7) and (18). Analytical solutions using a Lagrangian coordinate are no longer possible. Numerical results are shown by the dashed curves in Fig. 4. They have been computed for an entrainment coefficient of $C_E = 0.02$, which is a significant entrainment but still clearly smaller than the assumed detrainment of $C_D = 0.05$, in qualitative accordance with Baines (2001, 2005). The main characteristics of the solution are unchanged and show the development of a near-isothermal layer. Entrainment reduces the negative buoyancy of intrusion air, so that the LNB is slightly higher than without entrainment. There is a relative shift of the intrusion cooling from lower to higher levels.

c. Extension of simplified topography to three dimensions

How does the evolution of the profiles change if a three-dimensional situation is considered instead of the two-dimensional geometry shown in Fig. 2? We keep the vertical sidewalls but we are now considering a cylindrical basin. As illustrated in Fig. 5, the total inflow of $U_{IN}D_{IN}L = M_{IN}L$ is distributed over an area of $L^2\pi/4$ so that the vertical velocity at the basin rim is

$$w_{IN} = \frac{4}{\pi}\frac{M_{IN}}{L}, \qquad (19)$$

which is larger than in the two-dimensional case [cf. (1)] by a factor of $4/\pi \approx 1.27$. Equation (19) implicitly accounts for the azimuthal cosine dependence of cross-rim flow. Thus, the two-dimensional results apply to the three-dimensional, rotationally symmetric case as well, but for a somewhat reduced inflow. What we are neglecting here are possible disturbances of the mesoscale flow due to the presence of the basin, such as a "collecting" effect that would cause streamlines to converge or, as in the case of the Meteor Crater, deflections caused by the basin rim. Also, the central part of the inflow, which hits the rim head-on, may be able to lift a deeper layer of cold air over the rim and into the crater than the parts that impinge at the sides. This is considered in section 3f. However, if we are not concerned with the detailed distribution of the inflow along the rim we can implicitly regard M_{IN} as a suitable average volume flux per unit width, which multiplied with L gives the total inflow.

d. Combined intrusion and in situ cooling for realistic topography

Another step toward realism is to replace the vertical sidewalls of the cylindrical basin by the actual area–height distribution of the Meteor Crater, derived from a high-resolution digital elevation dataset. The two main
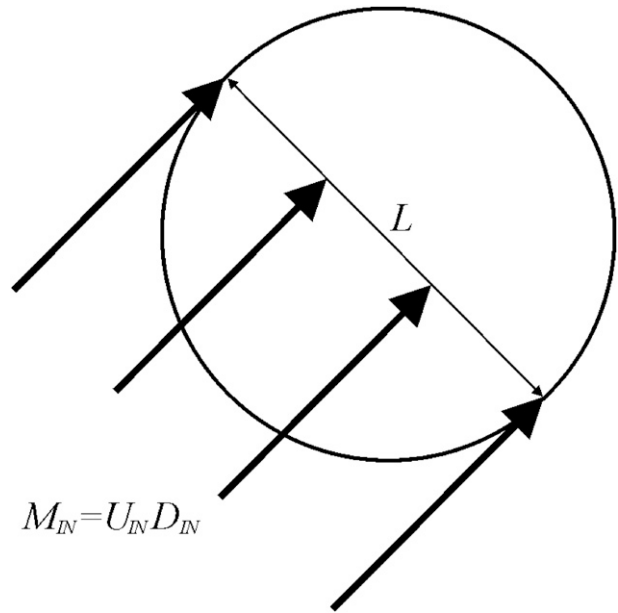

FIG. 5. Schematic depiction of the cold-air inflow for 3D geometry.

effects of this modification are a reduction of total air volume in the Meteor Crater compared to the cylindrical basin by ~40%, and the fact that, due to the reduced cross-sectional area, a given vertical mass flux is equivalent to a higher vertical velocity at lower levels where the basin is less wide. Figure 6 shows the resulting temperature evolution for an inflow speed of 2 m s^{-1}. As in the vertical sidewall case, a quasi-linear profile develops. The speed of formation is increased in accordance with the reduced volume of the crater compared to the cylindrical basin. The quasi-linear stratification, which is completely established after 2 h of inflow, is now, however, closer to dry-adiabatic than to isothermal.

e. Physical significance of the near-isothermal stratification

If there were no detrainment, what would determine the temperature gradient of the quasi-linearly stratified air in the crater above the undisturbed surface layer? In our model it is the result of two competing processes, of which one tends to produce a neutral stratification (adiabatic lifting), and the other tends to increase stability (continuous cooling of the air coming over the crater rim). The second process is due to the fact that over time, colder and colder intrusion air enters the crater. The rate of this external cooling, as can be seen from the spacing of the quasi-linear profiles in Fig. 6, is $-\partial\theta_{IN}/\partial t \approx 1$ K h^{-1}. The intrusion process translates this into a vertical gradient,
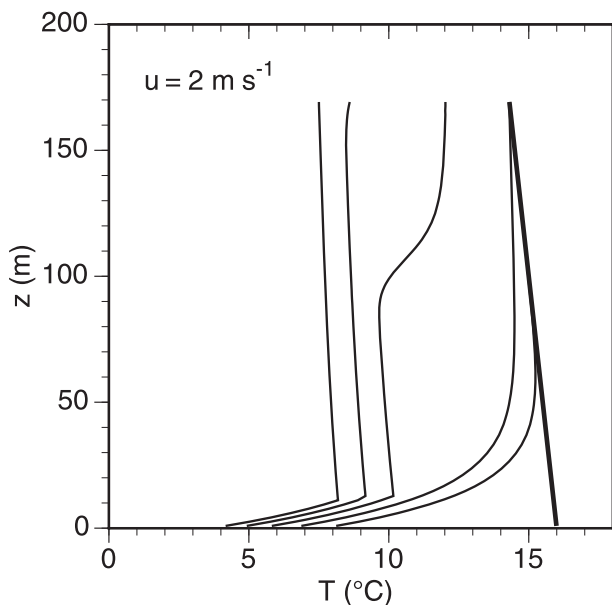
FIG. 6. Time evolution of temperature for a realistic volume–height distribution of the Meteor Crater and an inflow speed of 2 m s^{-1}. The value of the detrainment parameter is $C_D = 0.05$.

$$\frac{\partial \theta}{\partial z} = -\frac{1}{w}\frac{\partial \theta_{IN}}{\partial t} = -\frac{\pi}{4}\frac{L}{U_{IN} D_{IN}}\frac{\partial \theta_{IN}}{\partial t}, \quad (20)$$

where (15) has been used for the second equality. Using $L = 1200$ m, $U_{IN} = 2$ m s^{-1}, and $D_{IN} = 15$ m, we obtain $\partial \theta / \partial z \approx 0.009$ K m^{-1}, which is rather close to isothermal stratification. As the size of the crater increases, so does the stratification according to (20). This is because the longer turnover time means a larger "age" difference between the intrusion air at the top and at the bottom of the quasi-linear layer. Thus, while each individual parcel experiences the usual dry-adiabatic cooling as it rises, the slowness of the rising motion combined with the fact that colder and colder air is involved, produces a lapse rate that is slightly stable.

In order for the above line of reasoning to be valid, most of the intrusion cooling must take place through an adiabatic rising motion rather than direct detrainment. The numerical model results indicate that this is the case for values of the detrainment coefficient of ~0.05 or smaller. For larger detrainment coefficients, an adiabatic layer develops because the cooling at upper levels in the crater exceeds that at lower levels and leads to buoyancy-driven vertical mixing. The laboratory results of Baines (1999) on downslope flows into a stratified environment show that detrainment coefficients are typically <0.04, which would lend some support to this picture. However, the slopes in Baines' laboratory experiments are smooth and uniform, unlike the inhomogeneous and partially rugged surface of the Meteor Crater, which makes direct quantitative comparison difficult.

f. Azimuthal dependencies

In the real atmosphere, the air that enters the crater on the upwind side will be colder than the air at some distance along the perimeter. This is because the cross-rim flow component is largest on the upwind side; hence, the flow is able to lift air from relatively lower (potentially colder) levels up and into the crater. When air with a whole spectrum of temperature deficits enters the crater, the level of neutral buoyancy becomes an entire range of levels. Near the sides of the crater, the inflowing air will have only a small temperature deficit and will have already detrained at higher levels in the crater, whereas air at the upwind side will penetrate deeper and detrain closer to the crater floor.

We can use the mass flux model to assess what effect this buoyancy sorting has on the temperature evolution in the crater. Lacking detailed information about the along-rim dependence of temperature deficit of the inflowing air, we make the assumption that it follows a cosine law. Note that this is a cosine dependence in addition to the one of the cross-rim flow component, which has already been accounted for implicitly, leading to the factor $4/\pi$ in (19).

If azimuthal variations of inflow temperature are taken into account, (7) describing the cooling due to cold-air intrusions assumes the more general form

$$\frac{\partial \theta}{\partial t} = -\frac{\partial}{\partial z}\left\{\int_{-\pi/2}^{\pi/2} w'(\varphi, z)[\theta - \theta_{IN}(\varphi)]\, d\varphi\right\}, \quad (21)$$

where φ is the azimuth angle (we define $\varphi = 0$ as the upwind side) and

$$w'(\varphi, z) = \frac{2}{\pi}\frac{M_{IN}}{L}\cos(\varphi)\exp\left[\frac{C_D}{D}(z - H)\right] \quad (22)$$

is the contribution to the total vertical motion w of inflow entering over the infinitesimal rim sector $d\varphi$. It is the infinitesimal form of (6). If integrated from $-\pi/2$ to $+\pi/2$, (22) gives the total $w(z)$ as in (6), but with the additional $4/\pi$ factor of the circular geometry [cf. (19)]. Note that by using (21) and (22) we still treat w as a horizontally averaged quantity inside the crater, but explicitly take into account the covariation along the rim of inflow speed and temperature deficit. In the actual numerical computation, the integral in (21) is approximated by the sum over small (1°) angle increments.

Figure 7 illustrates the resulting temperature evolution. Comparison with Fig. 6 shows the expected reduction in the degree of cooling, since only the air impinging

perpendicularly onto the crater rim now has the maximum temperature deficit. Also, the characteristic filling-up signature of the intrusion cooling, which is evident in Figs. 4 and 6, is less pronounced. The temperature profile develops a stratification that is closer to isothermalcy than in the case without azimuthal variations. During the evolution toward the near-isothermal state, the stratification remains more uniform in the vertical because of the more distributed detrainment associated with buoyancy sorting.

g. Sinking of detrained air

Up to now it has been assumed that the detrained inflow air is mixed completely and instantaneously with the ambient air in the crater at the level of detrainment. In the real atmosphere, however, the mixing process takes a finite time, and as long as a detrained volume of air is still cooler than the ambient air, it will continue to sink. This is what has been observed in the laboratory experiments of Baines (1999, 2001, 2005). He describes three regions: (i) the actual downslope flow layer, (ii) a mixing region containing detrained fluid, and (iii) the undisturbed ambient fluid. The conceptual model depicted in Fig. 2 takes i and iii into account, but not ii. We now ask whether the presence of this additional region substantially alters the temperature evolution in the crater.

The net effect of taking the mixing region ii into account will be a stronger downward mass flux in the crater because parcels retain some of their negative buoyancy even after detrainment. This can be built into the mass flux model by adding to the downslope mass flux $M(z)$ as given by (5) an additional downward mass flux $N(z)$. It is important to note that the additional mass flux cannot be prescribed independently but follows from the detrainment profile and from an assumption about the degree of mixing of the detrained air. We denote the degree of mixing by the parameter $0 \le \varepsilon \le 1$, which means that a mixture will consist of ε parts intrusion air and $1 - \varepsilon$ parts crater air. If $\varepsilon = 0$, there is complete instantaneous mixing, which leads back to the previous model. If $\varepsilon = 1$, there is no mixing, which means the detrained air sinks to the same level of neutral buoyancy as the air that has remained in the downslope flow. This is equivalent to having no detrainment at all, and hence also leads back to the previous model, for the special case $C_D = 0$.

Using again the two-dimensional framework, the governing equations assume the form

$$L \frac{\partial \theta}{\partial t} = -\frac{\partial}{\partial z}[(M + \varepsilon N)(\theta - \theta_{IN})], \qquad (23)$$

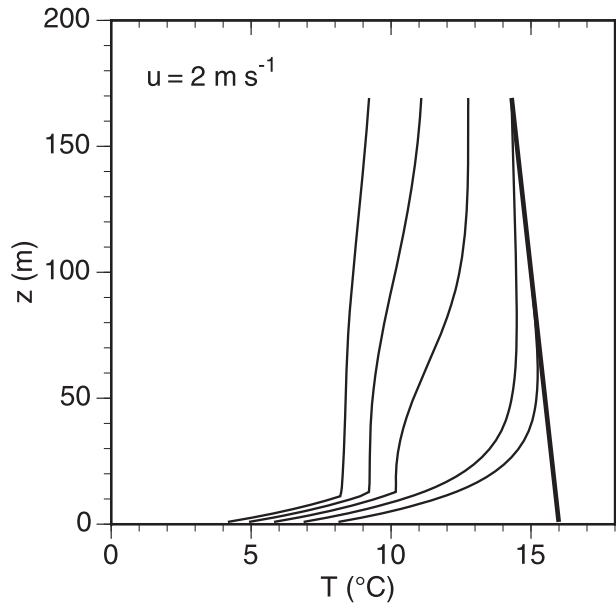$$N(z) = \int_z^{z_T} C_D U(z') \, dz', \qquad (24)$$

FIG. 7. As in Fig. 6, but with azimuthally varying inflow temperature.

where z_T is the uppermost level of origin of detrained air that can reach level z. This level is implicitly defined by

$$\theta(z_T) = \frac{\theta(z) - \varepsilon\theta_{IN}}{1 - \varepsilon}. \qquad (25)$$

In using (25), we set $z_T = H$ whenever $z_T > H$ because no detrained air is generated above the height of the crater rim. The physical process represented by (24) and (25) is that the sinking motion at a given level in the mixing region is the result of the sinking of all air parcels that were detrained between that level and the level z_T aloft. If the mixing is strong (ε small), detrained air cannot sink very far, so z_T, as implicitly given by (25), will only be slightly above the level z. The additional sinking motion is compensated for by the additional adiabatic rising motion in the crater.

What are realistic values for the mixing parameter ε? Visualization of the mixing region in the tank experiments of Baines (2005) shows that its depth is typically 5–10 times greater than the depth of the undiluted katabatic flow. Based on this we may assume that typical values for ε are in the range of 0.1–0.2. Figure 8 shows the temperature evolution for $\varepsilon = 0.2$ (dashed lines) compared to the reference case $\varepsilon = 0.0$ (continuous lines) that was already shown in Fig. 3c. The changes are rather subtle. It can be seen that the cooling is somewhat reduced in the uppermost layers, and slightly increased at heights between 100 and 150 m. The profiles are more linear, and the total amount of cooling is larger. This is
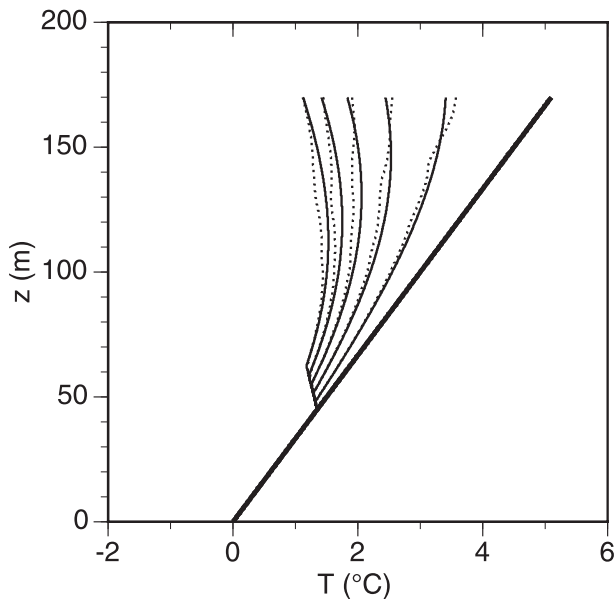
FIG. 8. Effect of sinking of detrained air in the case of intrusion-only cooling. Dashed curves show evolution of temperature profiles for a mixing parameter value of $\varepsilon = 0.2$. For comparison, the curves of Fig. 3c corresponding to $\varepsilon = 0$ are also shown (continuous lines).

because the temperature at the top remains a bit higher over the first several hours, keeping the temperature difference between inflowing and outflowing air somewhat higher.

4. Summary and conclusions

A mass flux model has been developed to explain the unexpected cooling behavior observed in Arizona's Meteor Crater. This cooling behavior, which differs from that found in other small basins, is characterized by the formation of a deep, near-isothermal layer above a shallow, stable surface layer. The conceptual model of cold-air intrusions proposed by Whiteman et al. (2010) is confirmed by the results of the mass flux model presented in this paper. The model also offers an explanation of the near-isothermal stratification in terms of increasingly colder intruding air and the finite time spent by air parcels in the compensating adiabatic rising motion. It has been shown that the detrainment parameter largely determines the characteristics of the cooling process, which may be described in terms of filling-up and "destabilization" modes. Through its effect on the shape of the temperature profile, the detrainment in a subtle way even affects the total cooling of the crater. An extended version of the mass flux model, which takes into account the sinking of detrained air, gives only slightly different results.

While the mass flux model has proven to be a useful tool for gaining a better understanding of the processes involved, its limitations in simulating the real atmosphere must be addressed. The main simplification is the treatment of in situ cooling, which has been prescribed based on observations and on conditions usually seen in other small closed basins. One possible approach would be to model the in situ cooling as part of the same mass flux framework since it leads to locally driven downslope flows. This could make the mass flux framework presented here useful for a wide range of applications (e.g., in the mapping of cold-air pooling potential). Another simplification concerns the fact that the model is essentially based on conservation of mass and heat but does not include the momentum budget. Hence, dynamic effects, such as the undershooting of intrusion air or the formation of gravity waves, are not taken into account. Nevertheless, the correspondence between model results and observations suggests that the most important processes have been captured.

Our modeling elucidates the physical processes that lead to changes in the initial temperature structure within a basin caused by cold-air intrusions over the basin rim. It should be noted that cold-air intrusions occur with other atmospheric phenomena in mountain areas (frontal passages, cold-air sources from adjacent watersheds, cloud waterfalls that form over ridges and passes, etc.). It is hoped that these initial simulations will provide an impetus to investigate other instances of the cold-air intrusion phenomenon.

REFERENCES

Baines, P. G., 1999: Downslope flows into a stratified environment - structure and detrainment. *Mixing and Dispersion in Stably Stratified Flows,* P. A. Davies, Ed., Oxford University Press, 1–21.

——, 2001: Mixing in flows down gentle slopes into stratified environments. *J. Fluid Mech.,* **443,** 237–270.

——, 2005: Mixing regimes for the flow of dense fluid down slopes into stratified environments. *J. Fluid Mech.,* **538,** 245–267.

Chow, F. K., A. P. Weigel, R. L. Street, M. W. Rotach, and M. Xue, 2006: High-resolution large-eddy simulations of flow in a steep alpine valley. Part I: Methodology, verification, and sensitivity experiments. *J. Appl. Meteor. Climatol.,* **45,** 63–86.

Clements, C. B., C. D. Whiteman, and J. D. Horel, 2003: Cold-air-pool structure and evolution in a mountain basin: Peter Sinks, Utah. *J. Appl. Meteor.,* **42,** 752–768.

De Wekker, S. F. J., and C. D. Whiteman, 2006: On the time scale of nocturnal boundary layer cooling in valleys and basins and over plains. *J. Appl. Meteor. Climatol.,* **45,** 813–820.

Eisenbach, S., B. Pospichal, C. D. Whiteman, R. Steinacker, and M. Dorninger, 2003: Classification of cold air pool events in the Gstettneralm, a sinkhole in the Eastern Alps. *Extended Abstracts Vol. A, Int. Conf. on Alpine Meteorology and MAP-Meeting 2003,* No. 66, Brig, Switzerland, MeteoSwiss, 157–160.

Emanuel, K. A., 1991: A scheme for representing cumulus convection in large-scale models. *J. Atmos. Sci.,* **48,** 2313–2329.

Fletcher, J. K., and C. S. Bretherton, 2010: Evaluating boundary layer–based mass flux closures using cloud-resolving model simulations of deep convection. *J. Atmos. Sci.,* **67,** 2212–2225.

Freytag, C., 1987: Results from the MERKUR experiment: Mass budget and vertical motions in a large valley during mountain and valley wind. *Meteor. Atmos. Phys.,* **37,** 129–140.

Haiden, T., and C. D. Whiteman, 2005: Katabatic flow mechanisms on a low-angle slope. *J. Appl. Meteor.,* **44,** 113–126.

Hourdin, F., F. Couvreux, and L. Menut, 2002: Parameterization of the dry convective boundary layer based on a mass flux representation of thermals. *J. Atmos. Sci.,* **59,** 1105–1123.

Mahrt, L., 1982: Momentum balance of gravity flows. *J. Atmos. Sci.,* **39,** 2701–2711.

Manins, P. C., and B. L. Sawford, 1979: A model of katabatic winds. *J. Atmos. Sci.,* **36,** 619–630.

Pinto, J. O., D. B. Parsons, W. O. J. Brown, S. Cohn, N. Chamberlain, and B. Morley, 2006: Coevolution of down-valley flow and the nocturnal boundary layer in complex terrain. *J. Appl. Meteor. Climatol.,* **45,** 1429–1449.

Reeves, H. D., and D. J. Stensrud, 2009: Synoptic-scale flow and valley cold pool evolution in the western United States. *Wea. Forecasting,* **24,** 1625–1643.

Savage, L. C., III, S. Zhong, W. Yao, W. J. O. Brown, T. W. Horst, and C. D. Whiteman, 2008: An observational and numerical study of a regional-scale downslope flow in northern Arizona. *J. Geophys. Res.,* **113,** D14114, doi:10.1029/2007JD009623.

Steinacker, R., and Coauthors, 2007: A sinkhole field experiment in the eastern Alps. *Bull. Amer. Meteor. Soc.,* **88,** 701–716.

Weigel, A. P., F. K. Chow, M. W. Rotach, R. L. Street, and M. Xue, 2006: High-resolution large-eddy simulations of flow in a steep alpine valley. Part II: Flow structure and heat budgets. *J. Appl. Meteor. Climatol.,* **45,** 87–107.

Whiteman, C. D., X. Bian, and S. Zhong, 1999: Wintertime evolution of the temperature inversion in the Colorado Plateau basin. *J. Appl. Meteor.,* **38,** 1103–1117.

——, T. Haiden, B. Pospichal, S. Eisenbach, and R. Steinacker, 2004: Minimum temperatures, diurnal temperature ranges, and temperature inversions in limestone sinkholes of different sizes and shapes. *J. Appl. Meteor.,* **43,** 1224–1236.

——, and Coauthors, 2008: METCRAX 2006: Meteorological experiments in Arizona's Meteor Crater. *Bull. Amer. Meteor. Soc.,* **89,** 1665–1680.

——, S. Hoch, M. Lehner, and T. Haiden, 2010: Nocturnal cold-air intrusions into a closed basin: Observational evidence and conceptual model. *J. Appl. Meteor.,* **49,** 1894–1905.

Zängl, G., 2005a: Dynamical aspects of wintertime cold-air pools in an Alpine valley system. *Mon. Wea. Rev.,* **133,** 2721–2740.

——, 2005b: Wintertime cold-air pools in the Bavarian Danube valley basin: Data analysis and idealized numerical simulations. *J. Appl. Meteor.,* **44,** 1950–1971.

Zhong, S., C. D. Whiteman, X. Bian, W. J. Shaw, and J. M. Hubbe, 2001: Meteorological processes affecting the evolution of a wintertime cold air pool in the Columbia basin. *Mon. Wea. Rev.,* **129,** 2600–2613.